



Edge and corner superconductivity in a two-dimensional topological modelYing Wang *Department of Chemistry, University of Southern California, Los Angeles, California 90089, USA*Gautam Rai *Department of Physics and Astronomy, University of Southern California, Los Angeles, California 90089, USA
and I. Institut für Theoretische Physik, Universität Hamburg, 22607 Hamburg, Germany*

Stephan Haas

*Department of Physics and Astronomy, University of Southern California, Los Angeles, California 90089, USA*Anuradha Jagannathan *Laboratoire de Physique des Solides, CNRS UMR 8502, Université Paris-Saclay, F-91405 Orsay Cedex, France*

(Received 17 October 2022; revised 22 December 2022; accepted 23 February 2023; published 13 March 2023)

We consider a two-dimensional generalization of the Su-Schrieffer-Heeger model which is known to possess a nontrivial topological band structure. For this model, which is characterized by a single parameter, the hopping ratio $0 \leq r \leq 1$, the inhomogeneous superconducting phases induced by an attractive- U Hubbard interaction are studied using mean-field theory. We show, analytically and by numerical diagonalization, that in lattices with open boundaries, phases with enhanced superconducting order on the corners or the edges can appear, depending on the filling. For finite samples at half filling, the corner site superconducting transition temperature can be much larger than that of the bulk. A novel proximity effect thus arises for $T_{c,\text{bulk}} < T < T_{c,\text{corner}}$, in which the corner site creates a nonzero tail of the superconducting order in the bulk. We show that such tails should be observable for a range of r and U values.

DOI: [10.1103/PhysRevB.107.104507](https://doi.org/10.1103/PhysRevB.107.104507)**I. INTRODUCTION**

In this paper, we consider the effects of attractive on-site interactions in a two-dimensional Su-Schrieffer-Heeger (2D SSH) model. This model is an extension of the well-known SSH chain [1,2] to two dimensions, with alternating weak (t_1) and strong (t_2) bonds along both spatial directions. In finite lattices, the noninteracting model has edge and corner modes in the appropriate topological sectors and is an example of higher-order topological insulators (HOTIs) [3]. Using the Bogoliubov–de Gennes formalism, we show that adding a Hubbard-type attractive on-site interaction results in a variety of inhomogeneous superconducting states in which the pairing is site dependent. Figure 1 shows examples of the possible different kinds of low-temperature superconducting phases—one can obtain phases for which the pairing order is quasi-one-dimensional [Fig. 1(a)], essentially restricted to the edges, is largest in the bulk and very small on the periphery [Fig. 1(b)], or is enhanced on the corner sites [Fig. 1(c)]. The spatial and thermal properties of these phases depend on the Hubbard interaction strength as well as on the ratio of hopping amplitudes of the model, $r = t_1/t_2$.

HOTIs have been much studied recently. The formation of electric multipole moments and charge pumping in such a lattice has been addressed [4,5]. Photonic systems based on the 2D SSH model were investigated in [6]. A classification scheme for topological superconductors and the

bulk-boundary correspondence in Bogoliubov–de Gennes-type models was discussed in [3,7,8]. In this paper we consider only the simplest possibility of s -wave pairing; however, we expect that similarly interesting edge and corner phenomena should appear when the basic model is extended to permit other types of superconducting pairing. The present study constitutes, for example, a good starting point for investigations of corner and edge Majorana fermions [9,10].

While edge modes and resulting higher-order topological superconducting phases have been reported before in the literature, as on the honeycomb lattice [11–13], the present model is of particular interest since it provides an analytically tractable example with a tunable parameter, whose ground state and finite-temperature properties can be described in detail. Furthermore, we observe an interesting interplay between surface and bulk superconductivity which has not been reported in HOTI structures so far.

This paper is organized as follows. In Sec. II we introduce the model, and the Bogoliubov–de Gennes (BdG) mean-field approach used here. In Sec. III we present results obtained by numerical diagonalization in 2D SSH systems. The dependence of local pairing order parameters on interaction strength, hopping ratio, and chemical potential is described. The critical temperatures of corner and bulk superconductivity are obtained. For a range of temperatures, a mixed state is shown to exist in open boundary condition (OBC) systems. Section IV presents a theoretical analysis, starting with the so-

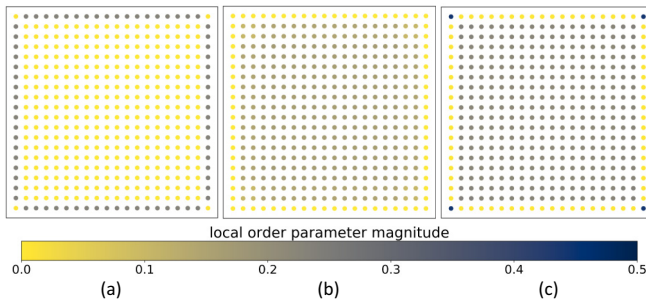


FIG. 1. Spatial variation of the local superconducting order parameters in a finite 2D Su-Schrieffer-Heeger lattice for different band fillings: (a) 1/4 filling (in the edge band), (b) 0.362 filling (in the central bulk band), and (c) 1/2 filling. The parameters used are $r = 0.1$ and $V = 1$.

lution for systems with periodic boundary conditions and then its generalization to topologically nontrivial finite systems. We conclude in Sec. V with a discussion and perspectives for future work.

II. ATTRACTIVE HUBBARD MODEL ON THE 2D SSH LATTICE

A. The noninteracting Hamiltonian

The 2D SSH tight-binding model is defined for sites lying on vertices of a square lattice of side a and involves two different nearest-neighbor hopping amplitudes, t_1 and t_2 . Along the horizontal (x) direction, the sequence of hopping amplitudes is alternating, just as in the parent one-dimensional (1D) SSH model [1,2]. The same is true for the hopping along the vertical (y) direction, as shown in Figs. 2(a) and 2(b). We will assume $t_1 \leq t_2$ and discuss properties of this model as a function of the hopping ratio $r = t_1/t_2 \leq 1$. The hopping

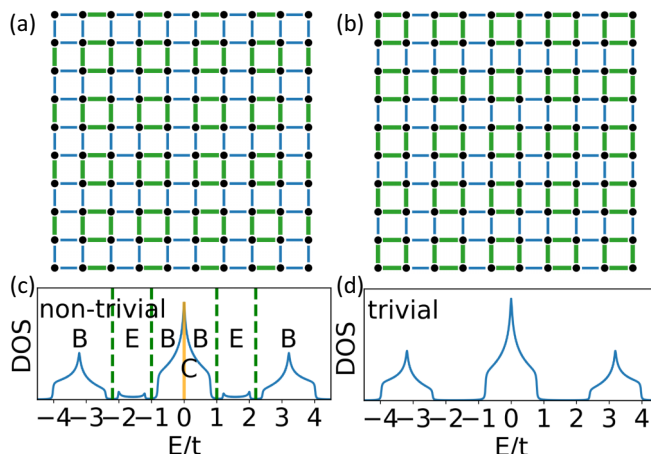


FIG. 2. Two finite systems showing (a) a nontrivial case and (b) the trivial case (black dots represent lattice sites, t_1 is represented by thin blue bonds, and t_2 is shown by thick green bonds). (c) DOS for the OBC nontrivial lattice. Bands in this DOS plot are labeled by B (bulk) and E (edge), and the peak at $E = 0$ includes a contribution C (corner). (d) DOS for the OBC trivial case. The PBC lattice has the same DOS as the OBC trivial lattice when the latter has enough unit cells. In these calculations, $r = 0.25$.

amplitudes are furthermore assumed to be positive (since the sign changes can be gauged away). The noninteracting Hamiltonian, discussed in detail in [14], is then

$$H_0 = - \sum_{\langle i,j \rangle} t_{ij} c_{i\sigma}^\dagger c_{j\sigma} + \text{H.c.}, \quad (1)$$

where $\langle i, j \rangle$ denote nearest-neighbor sites i and j and σ denotes spin. The unit cell consists of four sites. The infinite system or the finite system with periodic boundary conditions (PBCs) can be diagonalized by Fourier transforming. Note that the energy spectrum can be obtained very easily since the problem is separable in x and y variables, giving rise to two 1D SSH spectra. The 2D spectrum is just the direct sum of the energy bands of the 1D SSH model, $\epsilon_{1D}(k_x)$ and $\epsilon_{1D}(k_y)$. The wave functions are products of the 1D SSH wave functions, that is, $\psi(k_x, k_y) = \psi_{1D}(k_x)\psi_{1D}(k_y)$. The corresponding energy bands are given by

$$\epsilon_{2D}^{(n)}(k_x, k_y) = \pm \epsilon_{1D}(k_x) \pm \epsilon_{1D}(k_y), \quad (2)$$

$$\epsilon_{1D}(k) = t_2 \sqrt{1 + r^2 + 2r \cos 2ka}, \quad (3)$$

where the wave vectors lie in the Brillouin zone, $-\pi/2a \leq k_j \leq \pi/2a$ ($j = x, y$). See Appendix A for the k -space Hamiltonian and the band structure. The parameter determining the spectral properties is r , while t_2 serves only to set the global scale of energy. The four choices of sign in the above expression for ϵ_{2D} ($++$, $+-$, $-+$, $--$) correspond to four bands which we henceforth label by $n = 1, \dots, 4$. The two overlapping central bands ($n = 2, 3$, corresponding to $+-$, $-+$) intersect along the diagonals, where $\epsilon_{2D}^{(2)} = \epsilon_{2D}^{(3)} = 0$. They transform into each other under the mirror symmetries that exchange $k_x \leftrightarrow \pm k_y$. The energy spectrum is particle-hole symmetric as the model is bipartite. When $r < \frac{1}{2}$, a gap separates the lateral bands from the central bands. There are logarithmic Van Hove singularities at $\epsilon = 0$ and at the centers of the two lateral bands.

With OBCs, topologically protected states can arise at the edges depending on the bond configuration. We use the term “weak edge” when all sites lying on the edge are connected to the interior by weak bonds. This configuration results in the appearance of 1D edge modes, which have wave modulations along the edge but decay exponentially along the direction perpendicular to the edge. Where two weak edges meet, there is an additional “zero-dimensional” corner mode which is exponentially decaying in both directions. The localization length ξ is that of the edge states of the 1D SSH chain and depends on the hopping ratio, $\xi = 2a/|\ln r|$. A precursor of this 2D lattice, a ladder-type system of two coupled chains, was studied in [15,16].

The total densities of states (DOSs) of the finite nontrivial and trivial 2D SSH lattice are shown in Figs. 2(c) and 2(d), respectively. The nontrivial system has two supplementary bands corresponding to the quasi-1D edge modes. The spectrum has four gaps for small r , which close when $r = 1/3$. If present, each of the zero-dimensional modes localized on corners of the square contributes a delta function $\delta(E)$ to the density of states. As for the trivial system (no weak edges), we will not consider it any further since the edge and corner phenomena under discussion here are not present in this case.

In the interacting problem, an attractive on-site Hubbard term H_{int} is added to H_0 with

$$H_{\text{int}} = -V \sum_i \hat{n}_{i\sigma} \hat{n}_{i\bar{\sigma}} \quad (4)$$

($V > 0$), where $\hat{n}_{i\sigma} = c_{i\sigma}^\dagger c_{i\sigma}$ is the number of electrons of spin σ on site i and $\bar{\sigma}$ represents the opposite spin of σ . We assume that the instability of interest is the s -wave superconducting instability. In particular, at half filling, a competing charge density wave instability could exist but could be suppressed by doping or adding a small next-nearest-neighbor hopping. To proceed, we use a standard mean-field approximation to write the following effective total Hamiltonian:

$$H_{\text{BdG}} = \sum_{i\sigma} (u_i^{\text{HF}} - \mu_i) c_{i\sigma}^\dagger c_{i\sigma} - \sum_{\sigma} \sum_{\langle i,j \rangle} t_{ij} (c_{i\sigma}^\dagger c_{j\sigma} + \text{H.c.}) + \sum_i (\Delta_i c_{i\uparrow}^\dagger c_{i\downarrow}^\dagger + \text{H.c.}), \quad (5)$$

where μ_i is the chemical potential. The mean fields are the Hartree-Fock shift $u_i^{\text{HF}} = -V \langle c_{i\uparrow}^\dagger c_{i\uparrow} \rangle$ and the (real) local superconducting order parameters (OPs) $\Delta_i = V \langle c_{i\uparrow}^\dagger c_{i\downarrow} \rangle$. These quantities are determined self-consistently for different choices of band filling and boundary conditions. They are site independent in the infinite lattice and in finite systems with periodic boundary conditions but become site dependent when there are edges.

III. NUMERICAL RESULTS

A. Order parameter results

We now present numerical solutions of the BdG equations for finite 2D SSH samples. The real-space method used to solve Eq. (5) was originally developed to study the inhomogeneous superconducting state in disordered systems [17]. It has also been applied to study periodic systems such as the checkerboard Hubbard model [18]. The calculation determines the pairing order parameter Δ_i for each site self-consistently as follows: an initial ansatz is made for the BdG Hamiltonian using randomly chosen values for the OPs $\Delta_i^{(0)}$. The Hamiltonian is diagonalized numerically to find the eigenvalues E_ζ and corresponding eigenvectors $\{u_\zeta, v_\zeta\}$. New values of Δ_i are computed using the expression

$$\Delta_i^{(1)} = V_i \sum_{\zeta} v_{i\zeta}^* u_{i\zeta} [1 - 2f(E_\zeta, T)], \quad (6)$$

where $f(E_\zeta, T)$ is the Fermi-Dirac distribution. These $\Delta_i^{(1)}$ are injected back into the BdG Hamiltonian, and the calculation is iterated until convergence is reached. The calculations have been done under a fixed bandwidth condition; that is, we vary the hopping ratio r while keeping the bandwidth $W = 2(t_1 + t_2) = 4t$ constant. Results are reported in units of t , the average hopping amplitude.

In Fig. 1 we illustrate the local OP distribution for different band fillings in a 20×20 lattice subjected to OBCs, with $r = 0.1$ and $V = 1$. Note that in all the open systems considered, all four edges are taken to be weak edges. Defining the total filling $\langle n \rangle = \frac{1}{N_{\text{sites}}} \sum_i \langle c_i^\dagger c_i \rangle$, Fig. 1(a) correspond to the

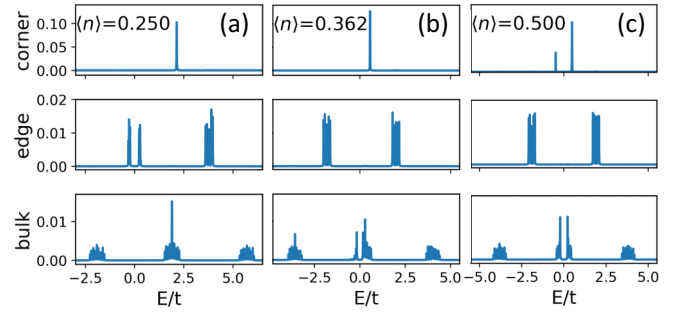


FIG. 3. Plots of the LDOS of corner, edge, and bulk sites for different band fillings. The parameters used are $r = 0.1$ and $V = 1$.

edge band being half-filled or the system being quarter-filled ($\langle n \rangle = 0.25, \mu = 1.90t$). Here, the OP is largest on the edges and decays exponentially into the interior, as we will show later. In Fig. 1(b), the central bulk band is partially filled ($\langle n \rangle = 0.362, \mu = 0.19t$). The OP is accordingly largest in the bulk of the sample. In Fig. 1(c), the system is at half filling ($\langle n \rangle = 0.5, \mu = 0$). Here, the OP is strongest on the four corner sites, followed by the bulk, while the edges have negligibly small OP. The local densities of states (LDOSs) for these three band fillings on the corner, edge, and bulk sites are shown in Fig. 3. These plots rationalize the site-dependent superconductivity pattern. The gap in the LDOS is seen only at the edge sites in Fig. 3(a), the bulk sites in Fig. 3(b), and both corner and bulk sites in Fig. 3(c). The most interesting situations, corresponding to the cases in Figs. 3(a) and 3(c), are discussed below.

1. Chemical potential at the band center (half filling)

In Fig. 4, we plot $T = 0$ order parameters as a function of V for several values of the hopping ratio r . The system sizes are large enough that the results have converged, and the error bars are smaller than the size of the symbols used in the plots. Figure 4(a) shows the quantity Δ_{bulk} defined as the value of the OP at one of the four equivalent central sites of the sample. For comparison, we also show values of the order parameter computed for PBCs Δ , which, of course, is independent of the position. At half filling, we note that, as the hopping ratio r increases from 0 to 1, Δ_{bulk} decreases. Figure 4(b) shows

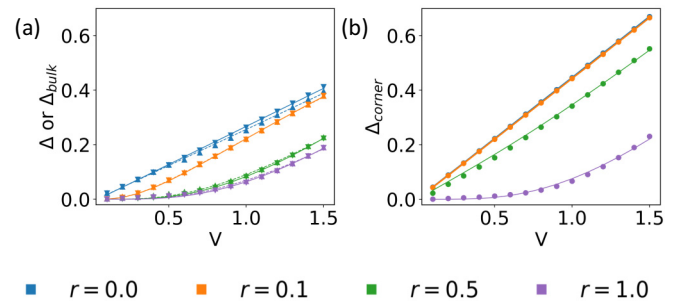


FIG. 4. Plots of the $T = 0$ order parameters versus V with fitting curves. (a) Δ for PBC (upward triangles with dashed line) and Δ_{bulk} for OBC (downward triangles with solid line); (b) Δ_{corner} for OBC (circles with solid line). Points indicate numerical results, and the solid lines are fits to the analytical expressions (see text).

TABLE I. Values of fitting parameters for zero-temperature corner site order parameters $\Delta_{\text{corner}}(0)$ fit to the function $f(V)$ for different r .

	r				
	0.0	0.1	0.5	0.9	1.0
$\Delta_{\text{corner}}(0)$					
c_1	0.44	0.44	0.32	0.04	0
c_2	0	0.02	4.96	23.32	26.27
c_3	0	8.33	28.96	34.40	34.27

Δ_{corner} defined as the value of the order parameter at one of the four (equivalent) corner sites. Figure 4 shows that, when $r = 0$, all of the order parameters are proportional to V . This is due to the form of the density of states, which is sharply peaked around $E = 0$, as explained in Sec. IV. In contrast, for r approaching 1, the order parameters vary as $\exp^{-\sqrt{c_3}/V}$, as obtained for the half-filled square lattice [19]. This type of scaling with V is expected when the Fermi level is located at a logarithmic Van Hove singularity [20,21]. For intermediate values of r the corner OP is well fitted by an extrapolation between the linear and exponential terms as follows:

$$f(V) = c_1 V + c_2 \exp^{-\sqrt{c_3}/V}. \quad (7)$$

Values of the fitted constants are given in Table I for each of the OPs. Note that c_2 vanishes when $r \rightarrow 0$, so that the variation is purely linear in V in this limit, while for $r = 1$, the linear term vanishes. These behaviors will be explained in Sec. IV.

2. Chemical potential in the edge band

When the chemical potential lies within the edge band (i.e., just above $\frac{1}{4}$ filling), a superconducting gap is opened in the edge band, as can be seen in Fig. 3(a). The spatial dependence of the order parameter is governed by the spatial properties of the 1D SSH edge modes, which are well known. One thus observes, in addition to the two-sublattice structure, an exponential decay of the order parameter as a function of the distance from the edge. Figure 5(a) presents a log-linear plot

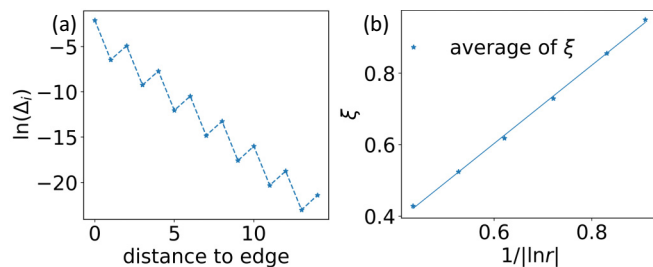


FIG. 5. (a) Plot of the log of the local order parameter $\ln(\Delta_i)$ versus distance to the edge under $V = 1$ and $r = 0.25$, showing the exponential decay and the odd-even oscillation (see text). (b) Plot of localization length ξ as a function of $1/|\ln r|$. The points show the values of ξ for different ratios of r , while the line shows the expected theoretical dependence. $r = 0.1, 0.15, 0.2, 0.25, 0.3, 0.333$ from left to right.

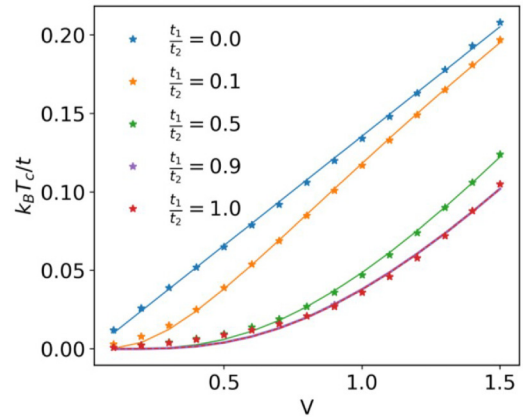


FIG. 6. PBC critical temperatures plotted vs V for ratio values of 0.0, 0.1, 0.5, 0.9, and 1.0.

of the local order parameter Δ_i versus the distance from the edge. Figure 5(b) shows the values of the fitted localization length ξ (points) of the exponential decay of Δ_i as a function of the hopping ratio r , along with the expected dependence given by $\xi = a/|\ln(r)|$ (line). We define Δ_{edge} as the local order parameter of one of the two equivalent sites at the center of one of the four equivalent edges. Finally, Δ_{edge} has the standard BCS dependence on V , namely, $\Delta_{\text{edge}} \sim \exp^{-c_3 t/V}$.

B. Finite-temperature results

Figure 6 shows results for the critical temperature of the periodic model at half filling $T_{c,\text{PBC}}$ plotted against V for different choices of the hopping ratio. Lines are fits to the data using the form $\exp^{-\sqrt{c_3 t}/V}$.

For OBCs and a range of r values, we find distinct transition temperatures for the bulk and corner OPs. This kind of two-step transition with corner (or surface) superconductivity followed by bulk superconductivity can be found more generally in systems with boundary surface states, as shown in [22–24]. The temperature dependence of the order parameter at bulk and corner sites, as well as for PBCs, is shown in Fig. 7 for $r = 0.5$ and $V = 1$. Figure 7 shows that the corner and

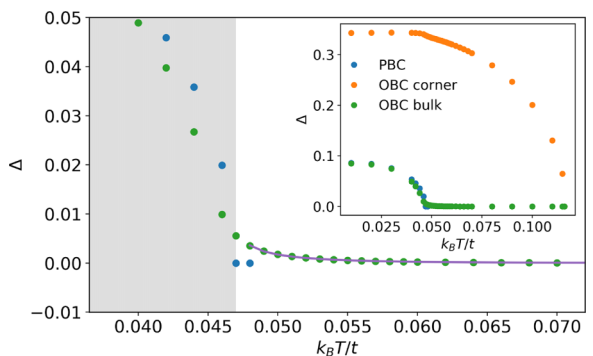


FIG. 7. Inset: T dependence of Δ_{corner} and Δ_{bulk} for OBC and of Δ for the $r = 0.5$ and $V = 1$ lattice. The main plot shows Δ_{bulk} versus T . The low-temperature region $T < T_{c,\text{PBC}}$ is shaded gray, and the tail of the bulk OP has been fitted to the expression given in the text.

bulk sites have different transition temperatures. The bulk OP, which is expected to go to zero at the bulk transition temperature $T_{c,\text{PBC}}$, actually shows a nonzero tail above this critical temperature. This tail arises from a proximity effect due to the corner site where the OP is still nonzero, and it accordingly vanishes when $T = T_{c,\text{corner}}$. One expects that the tail should be proportional to the corner OP and should also depend on R , the distance of the midpoint from the corner as $e^{-R/\lambda(T)}$. Here, $\lambda(T)$ is the correlation length. Close to the bulk transition the correlation length should vary as $\lambda(T) = A/\sqrt{T - T_{c,\text{PBC}}}$ in mean-field theory. In this formula the prefactor A depends on the hopping ratio, increasing monotonically as $r \rightarrow 1$. Indeed, as shown in Fig. 7, the tail is well fitted by this form. The tail is clearly visible only within a range of r values. For very small hopping ratios, the correlation length $\lambda(T)$ is too short for the tail to be observable. For larger $r \sim 1$, the correlation length is large, and corner and bulk critical temperatures are very close, so that no tail is observed.

IV. THEORETICAL ANALYSIS

A. Calculation for periodic boundary conditions

We begin by considering a translationally invariant 2D SSH square of side L with $N = (L/2a)^2$ unit cells, subject to periodic boundary conditions. Due to the lattice symmetries, all sites have the same order parameter, $\Delta_i = \Delta$. We outline the gap equation that is obeyed in the particle-hole-symmetric half-filled lattice, $\mu = 0$. We will consider the weak-coupling limit and small V and define the expectation values $b_{\vec{k}}$ by

$$b_{\vec{k}}^{(n)} = \langle \eta_{\vec{k}\downarrow}^{(n)} \eta_{-\vec{k}\uparrow}^{(n)} \rangle, \quad (8)$$

with all other expectation values of two annihilation operators assumed to vanish by the symmetries of the problem. $\eta_{\vec{k}\sigma}^{(n)}$ are eigenmodes in Fourier representation. The order parameter Δ can be written in terms of a sum over bands using the transformation to the diagonal basis. One has $\Delta = \sum_n \Delta^{(n)}$, where

$$\Delta^{(n)} = \frac{V}{4N} \sum_{\vec{k}} b_{\vec{k}}^{(n)}. \quad (9)$$

One can additionally simplify by assuming that only the two central bands contribute and fix the band index at $n = 2$ (it suffices to keep only one of the two central bands in the sums over \vec{k} by virtue of their symmetry under the exchange of k_x and k_y). The BdG equations for different \vec{k} decouple, giving rise to 2×2 matrices of the form

$$H_{\vec{k}} = \begin{pmatrix} \epsilon_{2D}(\vec{k}) & \Delta \\ \Delta & -\epsilon_{2D}(\vec{k}) \end{pmatrix}, \quad (10)$$

where $\epsilon_{2D}(\vec{k})$ is given by Eq. (2). Diagonalization yields quasiparticle energies of the form $E(\vec{k}) = \sqrt{\epsilon_{2D}^2(\vec{k}) + \Delta^2}$. As in the standard case, the gap equation is obtained from the self-consistency condition, which reads

$$\Delta(T) = \frac{V}{2} \int d\epsilon \rho(\epsilon) \frac{\Delta(T)}{E} \text{th}(\beta E/2), \quad (11)$$

where $\beta = 1/k_B T$ is the inverse temperature and $\epsilon = \epsilon_{2D}$ is the single-particle energy. This gap equation predicts that, for

fixed V , the order parameter $\Delta(0)$ decreases as a function of r . In particular, for small r , perturbative expansion predicts a decrease of the OP proportional to r^2 . This is, indeed, seen in Fig. 4.

In the limit $r \rightarrow 0$, the gap equation can be solved to obtain the $T = 0$ order parameter $\Delta(0)$ as a function of V . As the width of the central band tends to zero, the DOS can be approximately replaced by a delta function $A\delta(E)$, where $A \approx 0.5$ is the fraction of states lying within this band (neglecting correction of the order of $1/L$). The gap equation yields $\Delta(0) \sim V$. The critical temperature can be determined from the gap equation from the requirement that $\Delta(T_c) = 0$. In the limit of small r , T_c scales similarly to the OP, that is, $T_c \propto V$.

For nonzero r the integral in Eq. (11) is determined by the logarithmic Van Hove singularity at $E = 0$. Instead of the standard BCS form, $T_c \propto \exp^{-1/N_0 V}$, that is expected for a regular density of states (where N_0 is the DOS at the Fermi level), the critical temperature here has a V dependence given by $T_c \sim \exp^{-\sqrt{cst}/V}$ [20,21]. These behaviors are confirmed by the numerical calculations, as shown in Fig. 6.

B. Calculation for open boundary conditions

Consider an open square sample of side L with two weak edges which meet at the corner situated at the origin. Thus, two perpendicular sets of 1D edge modes and one zero-dimensional corner mode are present, in addition to the bulk modes. The extension to situations with more than one corner mode is straightforward. To simplify the analyses, we will assume that the sample is large so that the number of bulk modes is much larger than the number of edge modes, which is smaller by a factor of $1/\sqrt{N}$. For convenience, we assign site index O to the corner site on the top left, site index B to the site in the middle of the 2D sample, and site index E to the central site of one of the two equivalent weak edges (the upper edge and the left edge). We will consider the superconducting OP at three specific locations as follows:

(i) For the corner site OP (site index $i = O$), $\Delta_{\text{corner}} = V \langle c_{O\downarrow} c_{O\uparrow} \rangle$.

(ii) For the OP at the bulk site(s) of the sample (site index $i = B$), $\Delta_{\text{bulk}} = V \langle c_{B\downarrow} c_{B\uparrow} \rangle$.

(iii) For the OP for a site at the midpoint(s) of a weak edge (site index $i = E$), $\Delta_{\text{edge}} = V \langle c_{E\downarrow} c_{E\uparrow} \rangle$.

Let ϵ_ν be the eigenvalues of the noninteracting Hamiltonian (1) and $\{\eta_\nu\}$ be the eigenmodes. We will suppose that they are ordered such that the first index $\nu = 1$ denotes the corner mode, followed by the edge modes denoted by $\nu = 2, \dots, 2L - 1$, and, finally, the 2D bulk modes ($\nu = 2L, \dots, L^2$). By diagonalization one obtains the transformation U which relates one from the real-space basis set $\{c_i\}$ to the expansion in a new basis $\{\eta_\nu\}$, i.e.,

$$c_j = \sum_\nu U_{j\nu} \eta_\nu, \quad \eta_\nu = \sum_i U_{\nu i}^{-1} c_i, \quad (12)$$

where $U^{-1} = U^T$, with the matrix U being real. The absence of translational symmetry makes it difficult to solve the coupled gap equations for OBCs. However, with simplifications, some limiting cases are solvable, as shown below.

1. System at half filling

In terms of the U transformation matrix, one can write the order parameter for the midpoint at $T = 0$, Δ_{bulk} , as follows:

$$\Delta_{\text{bulk}} = V \sum_{\nu \in \text{bulk}} U_{B\nu}^2 b_{\nu\nu}, \quad (13)$$

where contributions of expectation values $b_{\mu\nu} = \langle \eta_{\mu\downarrow} \eta_{\nu\uparrow} \rangle$ for $\mu \neq \nu$ are neglected. In the small- r limit, the corner mode contribution and edge mode contributions can be dropped—the former decays very fast and therefore is zero in the center of the sample, and the latter is very small because the edge band is far from the Fermi level. One has then

$$\Delta_{\text{bulk}} \approx \frac{V}{4N} \sum_{\nu \in \text{bulk}} b_{\nu\nu}, \quad (14)$$

where the sum is over the bulk modes $\nu \geq 2L$. In the equation above, we have simplified by replacing the coefficients $U_{M\mu}^2$ by their average value $\bar{U}^2 = 1/4N$. To compute $b_{\mu\mu}$, we assume that the interaction term can be decomposed into 2×2 blocks H_ν in the space $\{c_{\nu\downarrow}, c_{\nu\uparrow}^\dagger\}$, as in the periodic case. In the case of bulk modes, the energies ϵ_ν are essentially the same as the energies ϵ_{2D} in Eq. (2). As a result, one obtains the same gap equation as in Eq. (11). In conclusion, $\Delta_{\text{bulk}} \approx \Delta$, and the bulk OP is essentially the same as the order parameter found for PBCs.

One can proceed in a similar way for the corner site OP Δ_{corner} . One finds

$$\begin{aligned} \Delta_{\text{corner}} &= V U_{11}^2 b_{11} + V \sum_{\nu \in \text{bulk}} U_{0\nu}^2 b_{\nu\nu} + \dots \\ &\approx a_1 V + a_2 \Delta, \end{aligned} \quad (15)$$

where the numerical index of the corner site is 1 and Δ represents the bulk OP given by Eq. (11). In the second line, the coefficients $U_{0\nu}^2$ have been replaced by their average value, written as a_2/N , with $a_2 < 1$ being a constant of the order of 1. In addition, we used the result of the BdG Hamiltonian for the η_0 mode, which gives $b_{11} = 1$. The constant $a_1 = U_{11}^2$. Both the coefficients a_1 and a_2 depend on the hopping ratio.

When $r \rightarrow 0$, $a_1 \rightarrow \frac{1}{4}$, and $a_2 \rightarrow 0$. Then $\Delta_{\text{corner}} = V/4$. Similarly, in this limit, the critical temperature for the transition at the corner can be shown to scale as $T_{c,\text{corner}} \sim V$.

When $r \sim 1$, all coefficients of the U matrix are of the same order of magnitude, $O(1/\sqrt{N})$. In this case, bulk modes contribute to leading order to all Δ_i , while the corner and edge modes can be neglected. This results in bulk OP and corner OP of the same order of magnitude, and both are similar to Δ computed for the periodic case. This explains the results shown in Fig. 4 for the corner and bulk order parameters as a function of V for different hopping ratios r .

2. Chemical potential in an edge band

When the Fermi level lies within an edge band, the superconducting gap opens within this band. The edge mode contributions are the most important, and the OP is the largest on the edges. Writing out the expansion of Δ_{edge} , one has

$$\Delta_{\text{edge}} = V \sum_{\nu \in \text{edge}} U_{E\nu}^2 \langle c_{\nu\downarrow} c_{\nu\uparrow} \rangle + \dots, \quad (16)$$

where i is the index of the midpoint of a weak edge and the sum runs over the indices $\mu = 2, 2L - 1$. As before, we approximate the coefficients $U_{E\nu}^2$ by their average values. The equation can then be simplified to give the self-consistent equation for this OP at $T = 0$ as follows:

$$\Delta_{\text{edge}} \approx \frac{V}{4\sqrt{N}} \sum_{\nu} \frac{\Delta_{\text{edge}}}{\sqrt{(\epsilon_\nu - u_{HF\nu} - \mu)^2 + \Delta_{\text{edge}}^2}}. \quad (17)$$

In this expression, for small r the single-particle energies ϵ_ν are essentially the one-dimensional energies ϵ_{1D} written in Eq. (2). Qualitatively, the above equation predicts that when the chemical potential lies within this band, the solution for the OP is expected to have the usual BCS form [25]. The numerical results described in Sec. III are in good accord with the analysis given here.

V. CONCLUSIONS

We have presented a detailed study of the inhomogeneous superconducting states found in the 2D extension of the Su-Schrieffer-Heeger model. We have focused on topologically nontrivial finite systems, where edge modes give rise to corner and edge superconducting phases. The present model is of particular interest since it provides an analytically tractable example which can be solved in real space. We have discussed the band structure of the noninteracting model and solutions in some simple limits for the interacting model treated in Bogoliubov–de Gennes mean-field theory. Numerical solutions have been obtained for the full range of hopping ratio t_1/t_2 . Depending on the hopping ratio and the band filling, we showed that the critical temperatures for these transitions scale in different ways with the Hubbard interaction V . The dependence can be linear or vary as an exponential square root or follow the standard BCS form.

We have obtained the phase diagram of the superconducting phase and shown that an interesting mixed phase can occur above the bulk transition temperature T_c , in which the bulk can have a nonzero superconducting order induced by a proximity effect from the corners.

An interesting direction for future work consists of extending the length of the unit cell of the 1D chains used in defining the 2D model. One can get edge and corner modes in 2D systems by considering chains of period 3, following a $\{t_1 t_2 t_1\}$ sequence in the x and y directions. This is a member of a set of finite sequences which in the infinite limit give rise to the Fibonacci quasicrystal, known to host topological edge modes [26,27]. It is not difficult to generalize our model to three dimensions by taking a direct product of three orthogonal SSH chains, in which case, vertex edge, surface, and bulk modes should appear. Variants of the 2D SSH model in the presence of next-nearest-neighbor hoppings were recently considered experimentally [28–30] and theoretically [6,31]. As we discuss in the Appendix B, this term, when small enough, does not result in qualitative changes in the above findings.

The s -wave superconducting phases we considered here are topologically trivial. Introducing gauge fields or spin-orbit interactions are some means to induce topologically nontrivial superconducting phases, as in [32]. Adding spin-orbit

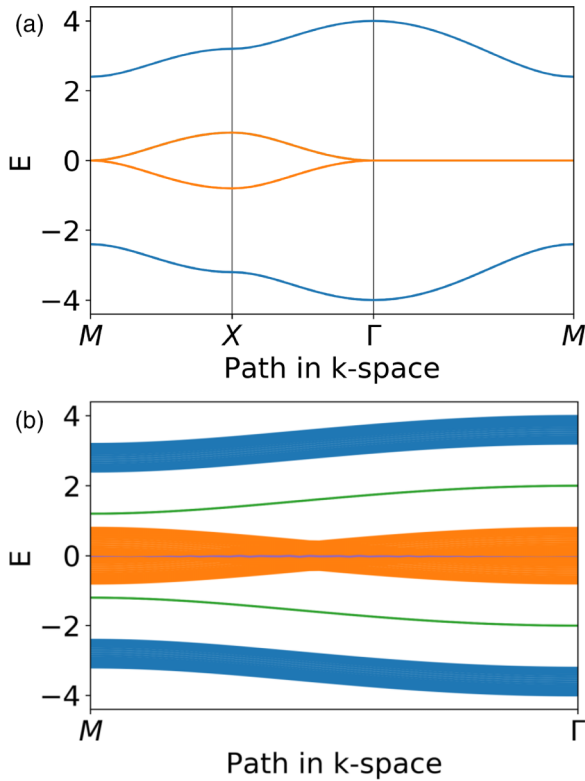


FIG. 8. (a) Band structure of the periodic 2D SSH model on a square lattice. Here, the high-symmetry points are $M(\frac{\pi}{2a}, \frac{\pi}{2a})$, $X(\frac{\pi}{2a}, 0.0)$, and $\Gamma(0.0, 0.0)$. (b) Band structure of the SSH model on a ribbon with periodic boundary conditions in one direction and open boundaries in the other direction. Here, the path in momentum space is one-dimensional, and the high-symmetry points are $\Gamma(0.0)$ and $M(\frac{\pi}{2a})$. We use $r = 0.25$.

interactions should lead to new interesting edge phenomena and competition between order parameters of different pairing symmetries close to the edges, as discussed in [33]. A recent paper introduced a route towards a 2D topological superconductivity starting from SSH chains [34]. In this work, however, boundary phenomena were not discussed, and it would be interesting to study their model predictions for finite samples. Last, but not least, Floquet topological systems such as those discussed in [35,36] constitute another class of systems likely to host interesting edge and corner superconducting states.

Future work will involve going beyond mean-field theory to investigate the stability of the low-dimensional phases described in this work. It will be interesting to see how the results are modified when fluctuations are included. It would be an interesting experimental challenge to realize edge and corner superconductivity. Two-dimensional SSH lattices could be realized by the bottom-up assembly of atoms, a method which has been used to fabricate “designer” structures, as described in [37]. Obtaining a 2D SSH lattice in the noninteracting limit should be possible, with the attractive Hubbard Hamiltonian being harder to obtain. If such a system is realized, electronic properties of the edge and corner superconducting phases could be probed by scanning tunneling spectroscopy.

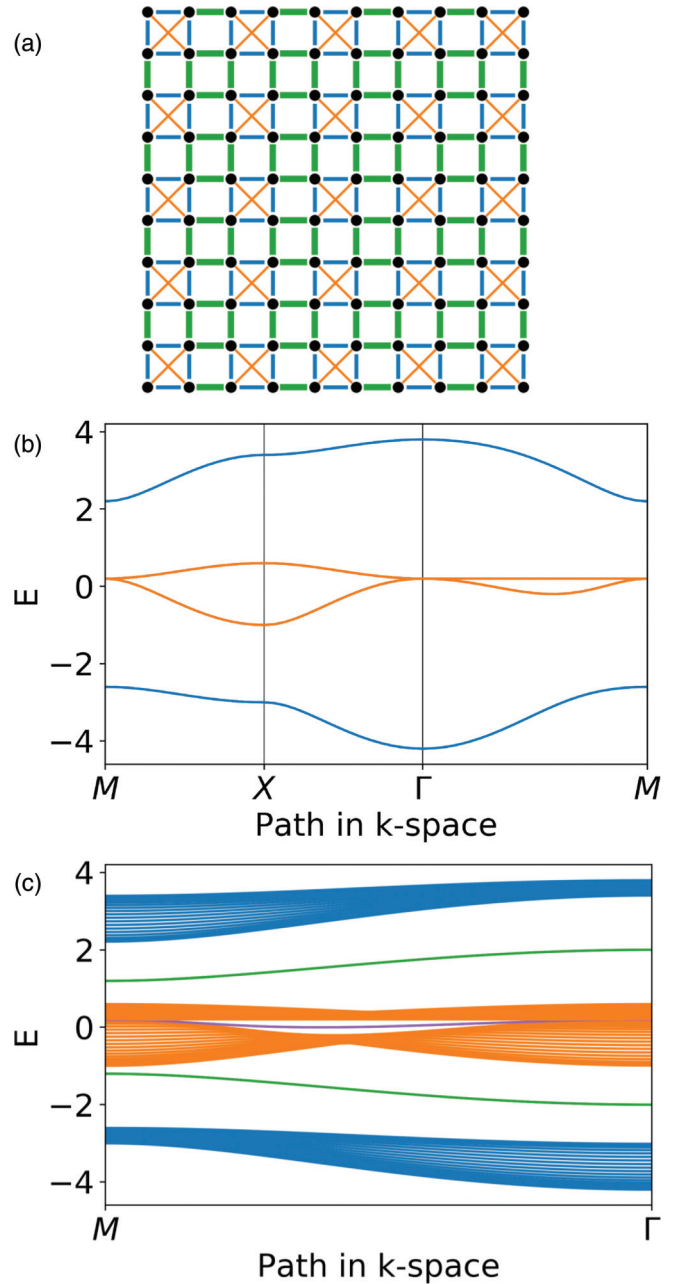


FIG. 9. (a) Illustration of the 2D SSH model, including intracellular next-nearest-neighbor hoppings. t_1 is represented by the thin blue bonds, whereas t_2 is depicted by the thick green bonds. The intracellular next-nearest-neighbor (NNN) hopping t_{NNN} is represented by the orange bonds. (b) Band structure of the periodic 2D SSH model with NNN hoppings. Here, the high-symmetry points are $M(\frac{\pi}{2a}, \frac{\pi}{2a})$, $X(\frac{\pi}{2a}, 0.0)$, and $\Gamma(0.0, 0.0)$. (c) Band structure of the 2D SSH model on a ribbon structure with NNN hopping. Here, we used $t_1 = 0.4$, $t_2 = 1.6$, and $t_{\text{NNN}} = 0.2$.

ACKNOWLEDGMENTS

The authors acknowledge the Center for Advanced Research Computing (CARC) at the University of Southern California for providing computing resources that have contributed to the research results reported within this publication.

APPENDIX A: MODEL ANALYSIS IN MOMENTUM SPACE

In each unit cell of the periodic lattice, we label the top left, top right, bottom left, and bottom right sites with a numerical index starting from 1. In momentum space, the noninteracting 4×4 matrix H_{momentum} is given by

$$H_{\text{momentum}} = \begin{pmatrix} 0 & \alpha(k_x) & \beta(k_y) & 0 \\ \alpha^*(k_x) & 0 & 0 & \beta(k_y) \\ \beta^*(k_y) & 0 & 0 & \alpha(k_x) \\ 0 & \beta^*(k_y) & \alpha^*(k_x) & 0 \end{pmatrix}. \quad (\text{A1})$$

Here, the matrix elements are

$$\alpha(k_x) = H_{12} = H_{34} = t_1 e^{ik_x a} + t_2 e^{-ik_x a}, \quad (\text{A2})$$

$$\beta(k_y) = H_{13} = H_{24} = t_1 e^{ik_y a} + t_2 e^{-ik_y a}. \quad (\text{A3})$$

In Fig. 8(a), the two orange dispersion curves correspond to the central bulk band in Fig. 2, whereas the blue dispersion curves belong to the two lateral bulk bands. When open boundary conditions are applied in one direction, as shown

in Fig. 8(b), two additional edge bands emerge, which are represented by the two green curves in Fig. 8. Furthermore, the flat purple band at energy 0 stems from the corner sites.

APPENDIX B: EFFECTS OF INTRACELLULAR NEXT-NEAREST-NEIGHBOR HOPPING

In order to make a comparison with recent experimental and theoretical work on related systems that include longer-range hopping [6,28–31], here, we consider the effects of two additional intracellular next-nearest-neighbor hopping matrix elements t_{NNN} . Comparing the band structures of the lattices in Figs. 8(a) and 9(b), the only qualitative difference is an asymmetry with respect to the dispersions of the top and bottom curves because next-nearest-neighbor hopping breaks the chiral symmetry and the particle-hole symmetry is lost. Furthermore, in Figs. 8(b) and 9(c), the two green edge bands and purple near-flat corner band still exist when introducing t_{NNN} . These features remain the same also when the two diagonal t_{NNN} 's are not equal to each other.

-
- [1] W. P. Su, J. R. Schrieffer, and A. J. Heeger, Solitons in Polyacetylene, *Phys. Rev. Lett.* **42**, 1698 (1979).
- [2] W. Su, J. Schrieffer, and A. Heeger, Erratum: Soliton excitations in polyacetylene, *Phys. Rev. B* **28**, 1138(E) (1983).
- [3] L. Trifunovic and P. W. Brouwer, Higher-order topological band structures, *Phys. Status Solidi B* **258**, 2000090 (2021).
- [4] W. A. Benalcazar, B. A. Bernevig, and T. L. Hughes, Electric multipole moments, topological multipole moment pumping, and chiral hinge states in crystalline insulators, *Phys. Rev. B* **96**, 245115 (2017).
- [5] W. A. Benalcazar, B. A. Bernevig, and T. L. Hughes, Quantized electric multipole insulators, *Science* **357**, 61 (2017).
- [6] X.-W. Xu, Y.-Z. Li, Z.-F. Liu, and A.-X. Chen, General bounded corner states in the two-dimensional Su-Schrieffer-Heeger model with intracellular next-nearest-neighbor hopping, *Phys. Rev. A* **101**, 063839 (2020).
- [7] M. Geier, P. W. Brouwer, and L. Trifunovic, Symmetry-based indicators for topological Bogoliubov–de Gennes Hamiltonians, *Phys. Rev. B* **101**, 245128 (2020).
- [8] X.-J. Luo, X.-H. Pan, C.-X. Liu, and X. Liu, Higher-order topological phases emerging from Su-Schrieffer-Heeger stacking, *Phys. Rev. B* **107**, 045118 (2023).
- [9] Y.-T. Hsu, W. S. Cole, R.-X. Zhang, and J. D. Sau, Inversion-Protected Higher-Order Topological Superconductivity in Monolayer WTe₂, *Phys. Rev. Lett.* **125**, 097001 (2020).
- [10] A. Jahin, A. Tiwari, and Y. Wang, Higher-order topological superconductors from Weyl semimetals, *SciPost Phys.* **12**, 053 (2022).
- [11] T. Li, M. Geier, J. Ingham, and H. D. Scammell, Higher-order topological superconductivity from repulsive interactions in kagome and honeycomb systems, *2D Mater.* **9**, 015031 (2021).
- [12] H. D. Scammell, J. Ingham, M. Geier, and T. Li, Intrinsic first- and higher-order topological superconductivity in a doped topological insulator, *Phys. Rev. B* **105**, 195149 (2022).
- [13] T. Li, J. Ingham, and H. D. Scammell, Artificial graphene: Unconventional superconductivity in a honeycomb superlattice, *Phys. Rev. Res.* **2**, 043155 (2020).
- [14] F. Liu and K. Wakabayashi, Novel Topological Phase with a Zero Berry Curvature, *Phys. Rev. Lett.* **118**, 076803 (2017).
- [15] K. Padavić, S. S. Hegde, W. DeGottardi, and S. Vishveshwara, Topological phases, edge modes, and the Hofstadter butterfly in coupled Su-Schrieffer-Heeger systems, *Phys. Rev. B* **98**, 024205 (2018).
- [16] S.-L. Zhang and Q. Zhou, Two-leg Su-Schrieffer-Heeger chain with glide reflection symmetry, *Phys. Rev. A* **95**, 061601(R) (2017).
- [17] A. Ghosal, M. Randeria, and N. Trivedi, Role of Spatial Amplitude Fluctuations in Highly Disordered *s*-Wave Superconductors, *Phys. Rev. Lett.* **81**, 3940 (1998).
- [18] K. Aryanpour, E. R. Dagotto, M. Mayr, T. Paiva, W. E. Pickett, and R. T. Scalettar, Effect of inhomogeneity on *s*-wave superconductivity in the attractive Hubbard model, *Phys. Rev. B* **73**, 104518 (2006).
- [19] J. E. Hirsch, Two-dimensional Hubbard model: Numerical simulation study, *Phys. Rev. B* **31**, 4403 (1985).
- [20] K. Noda, K. Inaba, and M. Yamashita, BCS superconducting transitions in lattice fermions, [arXiv:1512.07858](https://arxiv.org/abs/1512.07858).
- [21] K. Noda, K. Inaba, and M. Yamashita, Magnetism in the three-dimensional layered Lieb lattice: Enhanced transition temperature via flat-band and Van Hove singularities, *Phys. Rev. A* **91**, 063610 (2015).
- [22] A. Samoilenka and E. Babaev, Boundary states with elevated critical temperatures in Bardeen-Cooper-Schrieffer superconductors, *Phys. Rev. B* **101**, 134512 (2020).
- [23] A. Samoilenka, M. Barkman, A. Benfenati, and E. Babaev, Pair-density-wave superconductivity of faces, edges, and vertices in systems with imbalanced fermions, *Phys. Rev. B* **101**, 054506 (2020).
- [24] A. Benfenati, A. Samoilenka, and E. Babaev, Boundary effects in two-band superconductors, *Phys. Rev. B* **103**, 144512 (2021).
- [25] Note, however, that when the chemical potential is in the region of the square-root Van Hove singularities, the dependence of the OP on V should, in principle, be modified, with $\Delta_{\text{edge}} \sim \sqrt{V}$. However, the degeneracy of the edge bands (a factor of $1/L$

- smaller than that of the bulk) is too small for this effect to be of practical significance.
- [26] Y. E. Kraus, Y. Lahini, Z. Ringel, M. Verbin, and O. Zilberberg, Topological States and Adiabatic Pumping in Quasicrystals, *Phys. Rev. Lett.* **109**, 106402 (2012).
- [27] G. Rai, H. Schlömer, C. Matsumura, S. Haas, and A. Jagannathan, Bulk topological signatures of a quasicrystal, *Phys. Rev. B* **104**, 184202 (2021).
- [28] N. A. Olekhno, A. D. Rozenblit, V. I. Kachin, O. I. Burmistrov, A. A. Dmitriev, P. S. Seregin, D. V. Zhirihin, and M. A. Gorlach, Higher-order topological states in the extended two-dimensional SSH model and their electric circuit implementation, in *CLEO: QELS_Fundamental Science* (Optica Publishing Group, Massachusetts, 2021), p. FTu1M.5.
- [29] N. A. Olekhno, A. D. Rozenblit, V. I. Kachin, A. A. Dmitriev, O. I. Burmistrov, P. S. Seregin, D. V. Zhirihin, and M. A. Gorlach, Experimental realization of topological corner states in long-range-coupled electrical circuits, *Phys. Rev. B* **105**, L081107 (2022).
- [30] L. Qi, G.-L. Wang, S. Liu, S. Zhang, and H.-F. Wang, Engineering the topological state transfer and topological beam splitter in an even-sized Su-Schrieffer-Heeger chain, *Phys. Rev. A* **102**, 022404 (2020).
- [31] A.-L. He, W.-W. Luo, Y. Zhou, Y.-F. Wang, and H. Yao, Topological states in a dimerized system with staggered magnetic fluxes, *Phys. Rev. B* **105**, 235139 (2022).
- [32] T. Meng and L. Balents, Weyl superconductors, *Phys. Rev. B* **86**, 054504 (2012).
- [33] L. Lauke, M. S. Scheurer, A. Poenicke, and J. Schmalian, Friedel oscillations and Majorana zero modes in inhomogeneous superconductors, *Phys. Rev. B* **98**, 134502 (2018).
- [34] P. Rosenberg and E. Manousakis, Topological superconductivity in a two-dimensional Weyl SSH model, *Phys. Rev. B* **106**, 054511 (2022).
- [35] T. Nag, V. Juričić, and B. Roy, Hierarchy of higher-order Floquet topological phases in three dimensions, *Phys. Rev. B* **103**, 115308 (2021).
- [36] A. K. Ghosh, T. Nag, and A. Saha, Hierarchy of higher-order topological superconductors in three dimensions, *Phys. Rev. B* **104**, 134508 (2021).
- [37] A. A. Khajetoorians, D. Wegner, A. F. Otte, and I. Swart, Creating designer quantum states of matter atom-by-atom, *Nat. Rev. Phys.* **1**, 703 (2019).